Chapter 3 Health Area

# THERMAL STUDY OF NANOCOMPOSITES FOR MEDICAL APPLICATIONS

**José Luis Luna Sánchez[1], José Luis Jiménez Pérez[1*], Zormy Nacary Correa Pacheco[2], Omar Usiel García Vidal[1], Ruben Gutiérrez Fuentes[3], Genaro López Gamboa[4], Misha Jessica del Castillo Aguirre[1], Rigoberto Carbajal Valdez[5], Alfredo Cruz Orea[5]**

[1]Unidad Profesional Interdisciplinaria en Ingeniería y Tecnologías Avanzadas-Instituto Politécnico Nacional, Av. Instituto Politécnico Nacional No. 2580, Col. Barrio la Laguna Ticomán, Alcaldía Gustavo A. Madero, C.P. 07340, Ciudad de México, México.

[2]Centro de Desarrollo de Productos Bióticos-Instituto Politécnico Nacional. Centro de Desarrollo de Productos Bióticos. Carretera Yautepec-Jojutla, km. 6, Calle CEPROBI, No. 8, San Isidro, Yautepec, C.P. 62731, Morelos, México.

[3]Tecnológico Nacional de México Campus Toluca, dirección Avenida Tecnológico s/n. Colonia Agrícola Bellavista, Metepec, C.P. 52149, Estado de México, México.

[4]Instituto Tecnológico de Toluca, Avenida Tecnológico s/n. Colonia Agrícola. Bellavista, La Virgen, CP 52149 Metepec, Estado de México, México.

[5]Departamento de Física, CINVESTAV-IPN, Av. Instituto Politécnico Nacional, No. 2508, Col. San Pedro Zacatenco, 07360, Estado de México, México.

jimenezp1957@gmail.com

Luna Sánchez J. L., Jiménez Pérez, J. L., Correa Pacheco, Z. N., García Vidal, O. U., Gutiérrez Fuentes, R., López Gamboa, G. et al (2023 Thermal study of nanocomposites for medical applications. In E. San Martín-Martínez (Ed.). *Research advances in nanosciences, micro and nanotechnologies. Volume IV* (pp. 73-92). Barcelona, Spain: Omniascience.

## Abstract

Technological advances in stereolithography 3D printing have allowed the development of new composites. Nowadays the trend is toward composites containing nanostructures modifying their physicochemical properties while maintaining their processability. In this work, the elaboration and characterization of silver nanoparticles (AgNPs) and silver nanowhiskers (AgNWs) and its nanocomposites in an acrylic resin is presented. The AgNPs were synthesized using a green method from Jalapeño Chili (Capsicum Annuum var Annuum) extract. The AgNWs were synthesized using the polyol method. Complementary studies were carried out to determine morphology, functional groups, the crystalline structure and the plasmon resonance by transmission electron microscopy (TEM), Fourier transform infrared spectroscopy (FTIR), X ray diffraction (XRD) and UV-vis spectroscopy, respectively. The resin nanocomposites were formulated with AgNPs or AgNWs at different concentrations and their thermal diffusivity was measured by Thermal Lens (TL). On the other hand, using photoacoustic spectroscopy (PAS), the characteristic curing time of the nanoresins was determined. It was found an increase in thermal diffusivity and curing time with the increase in concentration of the nanostructures and higher curing time for the AgNWs nanocomposite. on the curing process. Samples were printed using SLA to find possible applications in 3D printing structures for medical application.

**Keywords:** 3D printing, nanocomposites, thermal properties, physicochemical characterization

## 1. Introduction

In the 80's a new manufacturing process to obtain solid prototypes from 3D digital images with relative high speed and ease of printing was developed. Layer by layer, thin films of a polymeric material, which is sensitive to UV light, are deposited. After the process is repeated many times, a solid piece of cured polymer is obtained, although curing time is short. Moreover, cost-energy savings are high and complex pieces can be obtained [1, 2].

Usually, the size of the printed objects is between 5-30 cm; therefore, to obtain pieces in the millimeter scale, is necessary to modify the printing technique. This also depends on the material to be used and the process itself. There main 3D additive manufacturing technologies are material extrusion, material jetting, Vat photopolymerization, powder bed fusion, sheet lamination, directed energy deposition, and binder jetting [3].

The additive manufacturing, 3D printing, or rapid modeling is focused on reducing printing time and improving the properties of the printed material. Among its advantages are speed is faster than other techniques, cheapness, complex geometries for printed pieces are obtained, higher availability, reduction of waste material.

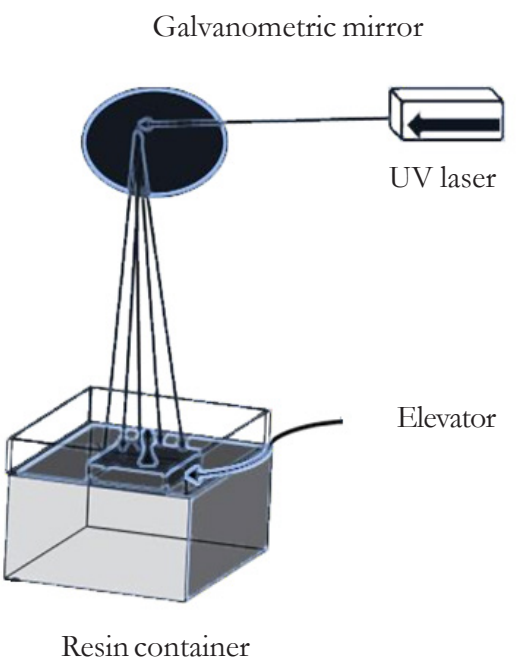


Figure 1. 3D printing by stereolithography.

On the other hand, among its disadvantages are limitations in materials used for printing, size limitation, accuracy, and is not possible mass production [4].

Among 3D additive manufacturing techniques, stereolithography (SLA) comes originally for lithography [5]. It uses the hydrophilic physical properties of a clay substrate on which the design is drawn with graphite. Due to the hydrophobic properties of graphite, the design is transferred from the clay plate to the substrate [6].

Nowadays, epoxy, vinyl or polyester resins are employed as well as bio-based resins based on starch, lactic acid or natural derivatives. In general, UV light and light-curing resins are used as shown in Figure 1. The laser light is directed by a galvanometric mirror which polymerizes the photocurable resin layer by layer by and UV laser, until the 3D figure is obtained.

The typical formulation for curing involves the use of a photo initiator, which generates the reactive species for starting the polymerization process, the monomers to be cured, and oligomers which can modify the structure of the resin [7]. The printed pieces currently have applications that range from biology to electronics and medicine [8]. The development of Nanotechnology has led the use resins in which nanometric-sized structures are incorporated, known as nanoresins or nanocomposites with the subsequent modification of the physicochemical properties of the final printed product. Metallic nanostructures such as Fe, Ti, Ag, Co and Au have been incorporated to polymers such as polyethylene and polylactic acid, among others. However, main problems faced up are poor incorporation of nanostructures into the polymer, agglomerations, changes in the size and shape of the nanostructures, before and during the polymer photocuring process [9].

Among photothermal techniques used to study the thermal properties and curing of resins used for 3D printing, photoacoustic (PA) and thermal lens (TL) are of special interest. In PA a beam of light in contact with a material causes a deformation on its surface with a subsequent expansion of the crystalline network and the release of energy in the form of waves in its surrounding environment. It is a sensitive and non-destructive technique. The experimental set up is shown in Figure 2. In this technique, a modulated beam of laser light hits the sample placed on a metal sheet generating thermal waves with pressure changes in the air adjacent to the metal sheet. Then, the acoustic signal produced is received by a microphone and sent to and amplifier for further processing [10 – 12].

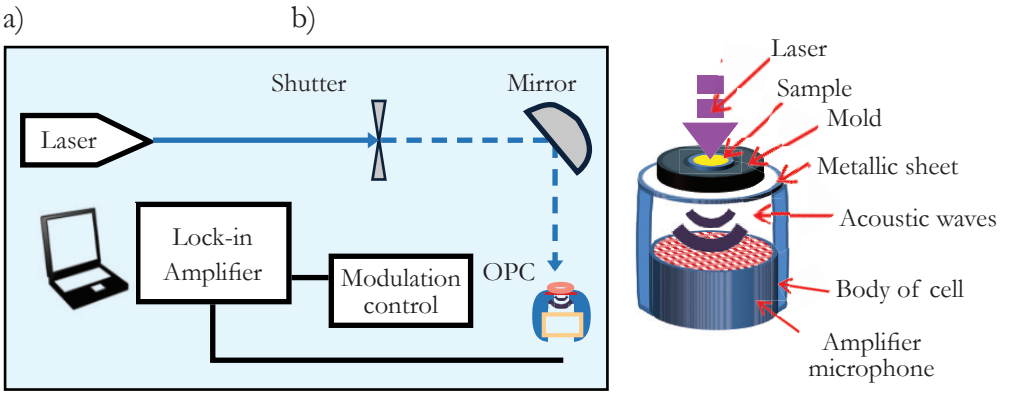


Figure 2. a) Experimental set up for PA. b) Open Cell Microphone (OPC).

Thermal lens (TL) is a phenomenon formed when a beam of laser light (pump laser) excites the sample. A second beam of laser light (probing laser) passes through that point being its trajectory modified due to the change in the refractive index caused by an increase in the temperature on the sample with respect to the surrounding environment [13 – 15]. The experimental set up is shown in Figure 3.

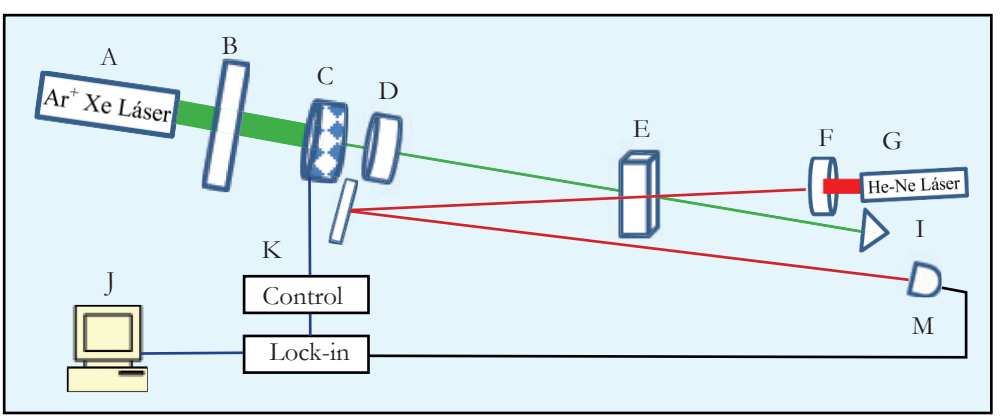


Figure 3. Experimental set up for TL: A) $Ar^+$ Xe ion pump laser, B) Filter, C) Shutter, D) Focusing lens 1, E) Liquid sample, F) Focusing lens 2, G) He-Ne probing laser, H) Mirror, I) Energy container, J) Computer, K) Shutter control, L) Lock-In, M) Detector.

The Fresnel theory as a function of time describes the TL phenomena as shown in Eq. 1.

$$I(t) = I(0) \cdot \left[ 1 - \frac{\theta}{2} \tan^{-1} \left( \frac{2 \cdot m \cdot V}{[(1+2 \cdot m)^2 + V^2] \cdot \frac{t_c}{2 \cdot t} + 1 + 2 \cdot m + V^2} \right) \right]^2 \quad (1)$$

being the probe laser beam at any time $t$. $I(0)$. is the initial value of $I(t)$ for $t$=0, $\theta$ is the shift of the phase in the probe beam after passing through the sample caused by the increase in temperature. $V=\left(\frac{z_1}{z_c}\right)$,$z_c$ is the confocal distance of the probe beam and $z_1$ is the distance from the probe beam waist to the sample. $\omega_p$ and $\omega_e$ are the beam spot sizes of the probe and excitation beams at the sample, respectively, $m=\left(\frac{\omega_p}{\omega_e}\right)^2$ and $\theta=-\frac{P_e \cdot A_e \cdot L}{k \cdot \lambda}\left(\frac{ds}{dT}\right)$, $P_e$ is the excitation beam power, is the optical absorption coefficient of the sample, $L$ is the sample thickness, $k$ is the thermal conductivity, $\lambda$ is the laser wave-length of the probe beam, and $\left(\frac{ds}{dT}\right)$ is the change of the optical path length with temperature of the probe beam. The characteristic time constant of the thermal lens is related to the thermal diffusivity as follows $D=\frac{\omega_e^2}{4 \cdot t_c}$ , in which $\theta$ and $t_c$ can be determined by fitting Eq. 1 to the experimental data obtained [16 – 18].

In this work, silver nanoparticles (AgNPs) and silver nanowires (AgNWs) were synthesized and added to an acrylic resin to elaborate and nanocomposite with possible applications in biomedicine. Samples were physicochemically characterized and thermal properties were measured.

## 2. Materials and methods

### 2.1. *Synthesis of nanostructures*

#### *2.1.1. AgNPs synthesis*

The methodology of Li *et al.* [19] was used for green synthesis of AgNPs from Capsicum annum L. extract (Jalapeño chili pepper). Chilis were bought at a local market in Mexico City. They were washed with distilled water. An extract was elaborated, centrifuged at 4000 rpm for 1 h and filtered. Later, the extract was made up to 250 mL in distilled water. As a precursor, 0.1 M of AgNO3 was used. Then, 10 mL of the precursor were added to 50 mL of the reducer at room temperature and stirred. Every hour (up to 11 h), a sample was taken, and absorbance was determined by UV-vis. Color changed from transparent to translucent white, reddish brown and finally dark cherry after 11 h of reaction time.

#### *2.1.2. AgNWs synthesis*

The AgNWs were synthesized using the polyol method [20]. Silver nitrate, glycerol and PVP were used as a precursor, solvent and reducer and protective agent were used. For that, 0.489 M of AgNO3 was dissolved in 19 mL of a

solution containing 0.284 mol of PVP in glycerol and stirred. On the other hand, 0.5 mL of a 2 M NaCl aqueous solution was dissolved in 1 mL of glycerol and homogenized. Both solutions were mixed and heated at 220 °C at a heating rate of 2.75 °C/min and stirred at 50 rpm. The reaction was stopped using deionized in a 1:1 ratio with respect to the volume of the reactant system and the resulting product was precipitated by centrifugation at 7000 rpm. The solids were washed with deionized water three times. Finally, the precipitate was dispersed in water for its characterization.

## 2.2. *Nanocomposites elaboration*

The AgNPs and AgNWs were added to an acrylic resin to form two different nanocomposites. For that, 1.5 to 6 mg of dry nanostructures were dispersed in 5 mL of the resin (INKTEK, Mexico) using and ultrasonic bath for 1 h. For further use as characterization and printing, the composites were homogenized in an ultrasonic bath for 30 minutes.

## 2.3. *Characterization*

### *2.3.1. Physicochemical characterization*

The UV-vis absorption coefficient was determined using a Genesis® 10S Spectrometer, in absorbance mode, range of 190-1100 nm, and a step of 5 nm. Functional groups were identified in a Bruker ® Alpha FTIR (Fourier Transformed Infrared Spectroscopy) equipment with a range of 400 – 4000 $cm^{-1}$ and a step of 2 $cm^{-1}$. Nanostructures' morphology was observed using a JEOL® JEM-1010 Transmission Electron Microscope (TEM) at an acceleration voltage of 60 kV. The X-ray diffraction (XRD) patterns were obtained using a Rigaku® Smart Lab diffractometer (Cu Kα, λ = 1.5418 Å), with a step of 0.02 °/s, and 2θ from 20-80°, voltage and current were 45 kV and 200 mA, respectively.

### *2.3.2. Thermal measurements*

2.3.2.1. Thermal diffusivity

Thermal diffusivity measurements of the nanoresin were carried out using the experimental set up shown in Figure 3. Briefly, the probing laser passes through the sample, reflects off the mirror and is directed towards the light intensity sensor. Then, the excitation laser beam penetrates in the interior of the liquid

sample, increasing the temperature in the surrounding medium, causing a deviation in its trajectory. Constant parameters used were Pe= 40 mW, (power of the Ar+Xe excitation laser at 514.5 nm (me= 4.9 ×10−3 cm the diameter of the excitation laser light beam; λp=632.8 nm (He-Ne probe laser wavelength), mp= 1.81 ×10−2 cm (probe beam diameter, red), m=13.691, V=1.22; zc=6.56 cm focal length; z1=2 m, L=1.0 cm (length of sample cell).

2.3.2.2. Curing time determination

The curing time was determined using the OPC set up shown in Figure 2. The liquid resin was placed inside a neoprene O-ring (5x2 mm) as a container on a metallic aluminum film (0.0012 mm thick). The sample was irradiated with a modulated laser beam at 17 Hz; with a wavelength of 400 to 450 nm and an average power of 2 mW. An Electret® microphone connected to the cell detects the wave generated due to temperature increase.

## 3. Results and discussion

### 3.1. *UV-vis of nanostructures resin and nanocomposites*

In Figure 4 the UV-vis of the resin with reaction time for the AgNPs can be seen. The curves show a band centered at 395nm, and an incipient growth of a band centered at 475 nm which corresponds to the surface plasmon resonance of silver. As the reaction progresses, the band at 475 nm is increased while the band at 395 nm is decreased. This behavior is like that reported by Li *et al.* [19].

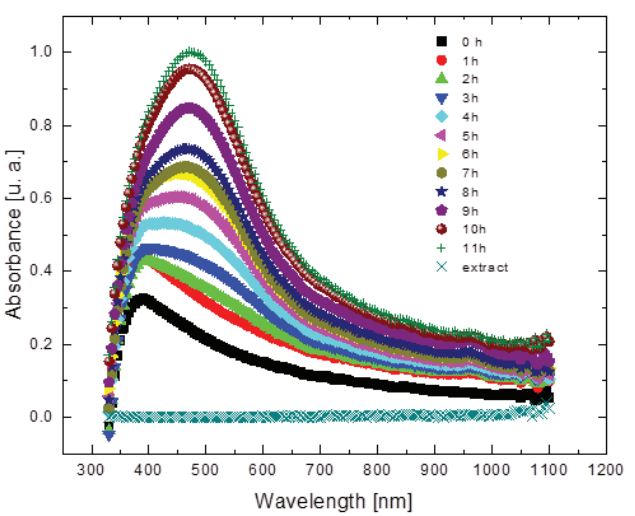


Figure 4. Kinetics of AgNPs synthesis followed by UV-vis spectrometry.

As seen in Figure 4 for AgNPs a main peak centered at 475 is observed because the vibrational mode is isotropic. On the other hand, AgNWs present two vibrational modes, one transversal and the other longitudinal corresponding to a shoulder centered at 350 nm assigned to transverse vibration and a band centered at 380 nm assigned to longitudinal vibration (spectra not shown) [21, 22].

In the UV-vis spectra of the acrylic resin (not shown) a band in the range from 277 to 429 nm was observed, the range in which the resin polymerizes.

For the nanocomposite, a band is observed from 420 to 435 nm (not shown), which remains in the same region, but changes slightly in intensity. The highest absorption started from 435nm and increases as the wavelength decreases.

### 3.2. *FTIR of nanostructures resin and nanocomposites*

In Figure 5, the FTIR spectra of the samples was taken every hour from the reacting system. All curves were similar. The characteristic absorption bands observed were at 3709-2803 $cm^{-1}$ for the symmetric and asymmetric vibration of the O-H bond and stretching vibrations of the N-H bonds of primary and secondary amines [23]. At 2816-1904 $cm^{-1}$, for water, corresponding to the symmetrical stretching of oxygen, -O- and the stretching of the S-H, NH2+, NH+ bonds, maybe from vitamins and thiols of the extract. The band at 1635 $cm^{-1}$ is related to the bending of the H-O-H bonds, to the amide bonds and to the C=O, -C=N bonds. Only small changes in the intensity of the band at 3709-2803 $cm^{-1}$ during the synthesis correlates with the kinetics found by UV-vis spectrometry in Figure 4. For AgNWs, the same peaks were observed (spectra not shown).

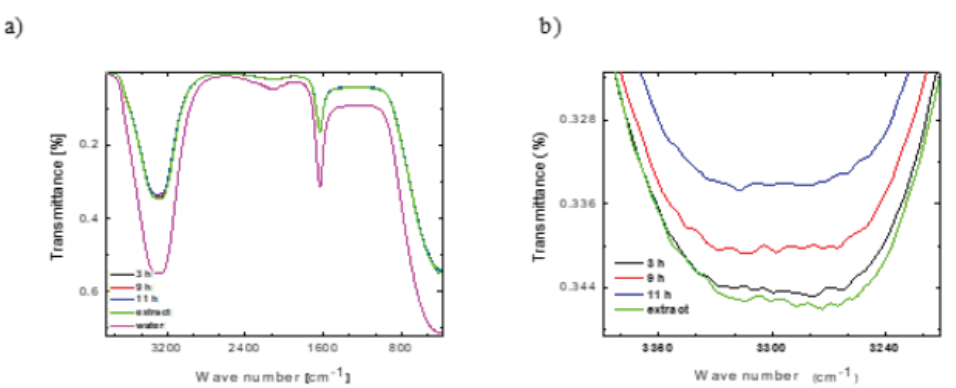


Figure 5. a) Kinetic monitoring of the synthesis of AgNPs.
b) Detail of the band at 3709-2803 cm-1.

The FTIR spectrum of the acrylic resin is shown in Figure 6. The most important absorption bands are 2869-2970 $cm^{-1}$ related to the stretching of the C-H bond (-$CH_3$ and -$CH_2$), at 1723 $cm^{-1}$ corresponding to the stretching of the C=O bond, a small band at 1635-1616 $cm^{-1}$ due to the stretching of the RCO-NH2 bond. At 1450 $cm^{-1}$, and a peak corresponding to the -CO-$CH_2$ bond. A broad band between 1016 and 1193 $cm^{-1}$, corresponding to the ester group and another broad band between 3600 and 3350 $cm^{-1}$ due to O-H stretching and amino group.

In the case of the nanocomposite, the FTIR spectra (not shown) had the bands corresponding to both, the nanostructures, and the resin.

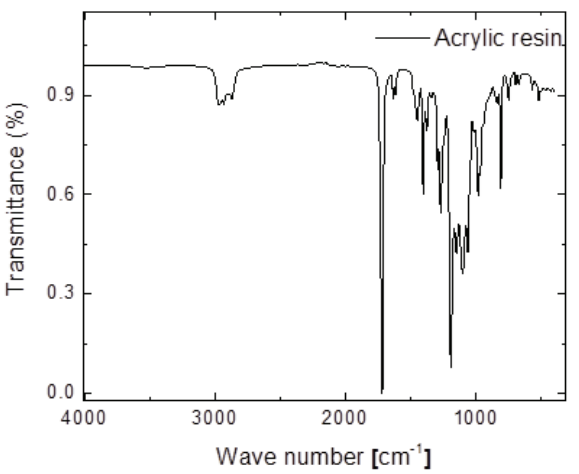


Figure 6. FTIR spectrum of the INKTEK acrylic resin

### 3.3. *TEM of nanostructures*

TEM images were used to determine the diameter of the AgNPs. The kinetics for 0, 5, and 11 h was observed. In Figure 7, a) an example of AgNPs at time 5 h is shown along with b) the particle size distribution histogram.

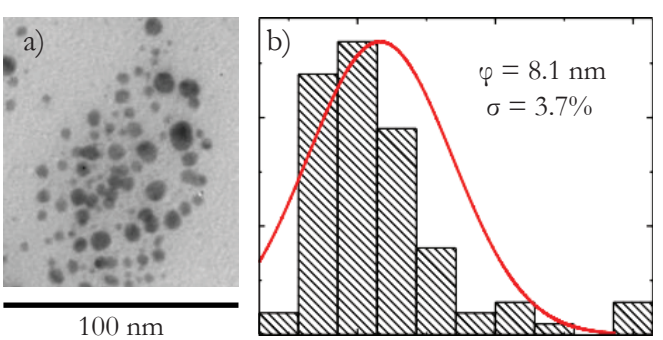


Figure 7. TEM images after 5 h reaction time for AgNPs synthesis.

The particles are spherical in shape and size distribution varies. In Table 1 the particle size for the different reaction times is shown.

Table 1. Particle diameter statistics.

| Particle size [nm] | | | |
|---|---|---|---|
| Time [h] | 0 | 5 | 11 |
| Minimun diameter | 2.5 | 2.9 | 5.9 |
| Maximum diameter | 12.7 | 21.3 | 35.8 |
| SD | 1.6 | 3.7 | 4.6 |
| Mean | 6.2 | 7.6 | 15.7 |

From TEM micrographs of AgNWs in Figure 8, linear, straight structures are observed, which different thickness and length (Figure 8a). No branches are observed. Considering these nanostructures as straight cylinders, the calculated diameter is 56.8 nm and the average length l=1451.7 nm with a mean aspect ratio of 25.6 (Figure 8b).

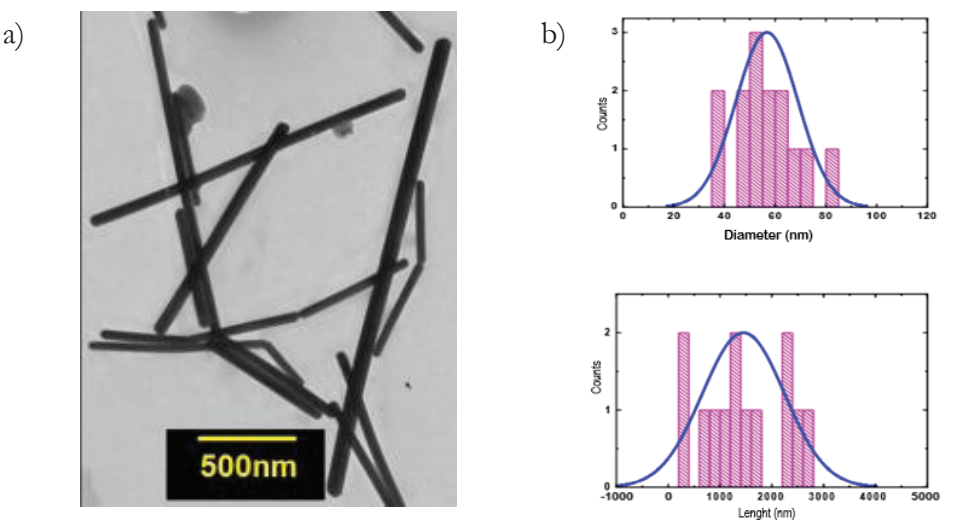


Figure 8. TEM images for AgNWs.

### 3.4. *XRD of nanostructures*

The structural properties of the AgNPs powders were analyzed by X-ray diffraction (diffractogram not shown). The obtained peaks corresponded to the planes of the cubic structure, FCC of silver [24], according to the Ag

crystallographic chart (JCPDS-ICDD chart04-0783) [25]. The peaks were observed at 37.8° corresponding to the (111) plane, at 45.9°, corresponding to the (200) plane, at 67.2 corresponding to the (220) plane, and at 76.5° corresponding to the (311) plane. Similar results were reported for AgNPs green syntheses using extracts of Santalum album fruits, Oryza Sativa seeds and Coleus aromaticus leaves [26].

For the AgNWs (diffractogram not shown), the signals corresponding to the FCC cell planes of silver were identified, which agree with the JCPDS standard file number 04-0783 of ASTM [27]. The crystallites that constitute them have a preferential orientation in the direction (111).

## 3.5. *Thermal properties of the nanocomposites*

### *3.5.1. Diffusivity of nanocomposites by TL*

In Figure 9 it can be seen that the thermal diffusivity of the nanocomposites increased as the concentration of nanostructures in the composite increased. For the same concentration, the thermal diffusivity of the AgNPs composites is higher than for the AgNWs nanocomposites due to the higher aspect ratio to volume of nanoparticles compared to nanowhiskers [28].

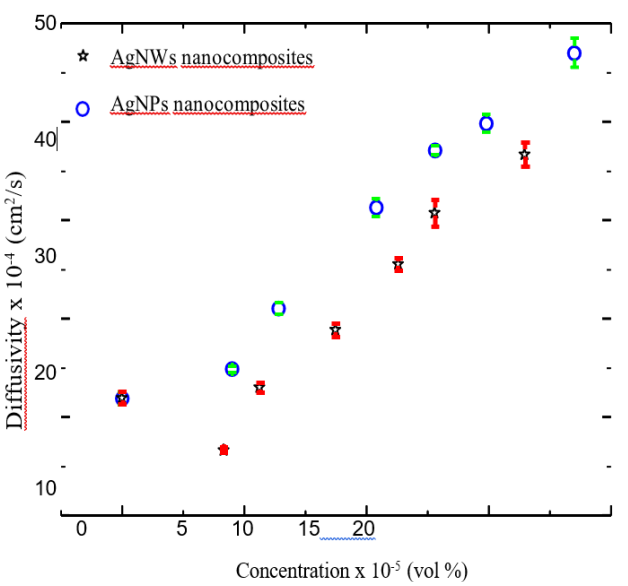


Figure 9. Thermal Diffusivity of the nanocomposites versus AgNPs or AgNWs nanostructures concentration (vol %) (in red and green the SD of the measurements).

### *3.5.2. Curing time of nanocomposites by PAS*

In Figure 10, the relationship between the AgNPs or AgNWs concentration and the characteristic curing time, τ. For the same concentration, it is observed that for the composites containing AgNWs the curing time is higher than for the nanocomposites containing the AgNPs. This may be due to the UV light with generates free radicals increasing the interfacial thermal resistance and then, curing time is higher [29]. Also, as concentration is increased, the curing time increased being more noticeable for the AgNWs. This increase is related to the number of reactive functional groups between the acrylic resin and the nanostructures. For lower nanostructures concentration, the characteristic time τ increases slowly. On the other hand, as concentration of nanostructures increased, the possibility of the reaction of these functional groups present on the surface of the nanostructures, increases the characteristic time τ [14].

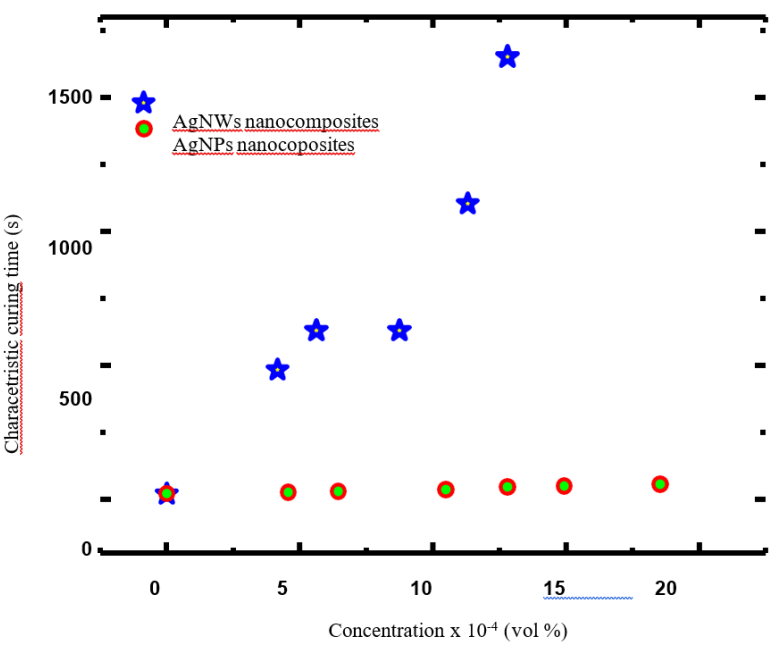


Figure 10. Characteristic curing time versus concentration for the nanocomposites.

### *3.5.3. SLA 3D Printing Process*

The composites formulated with the AgNPs and AgNWs were 3D printed in the form of meshes (1 $cm^2$) for application as cellular scaffolds. AN UV laser with a wavelength of 405 nm was used. The system was illustrated in Figure 1 and the interior of the printer is shown in Figure 11.

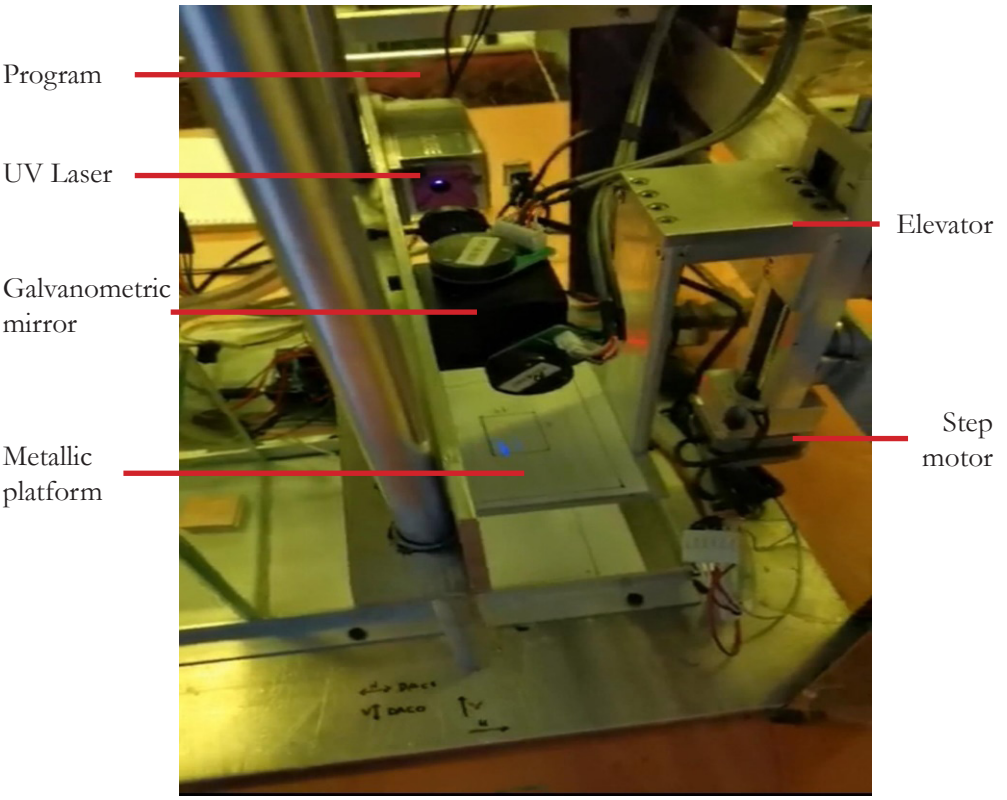


Figure 11. Inner part of the experimental 3D printer.

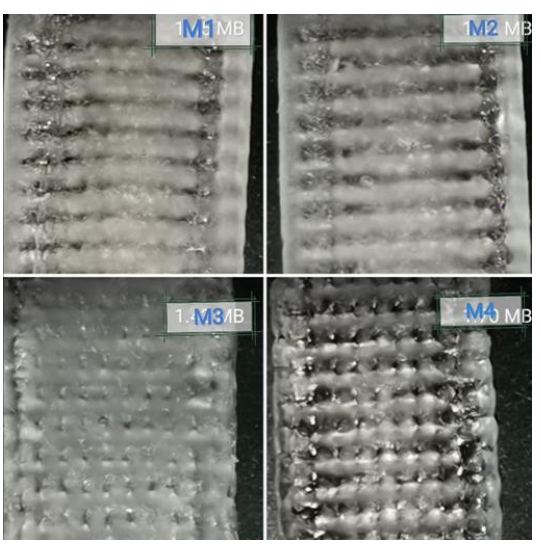


Figure 12. 3D printed structures.

The parameters considered for 3D printing are the numerical data to stablish the initial position of the laser, the height at which the printing starts, the total area of the printed mesh, the number, and the space between the vertical and horizontal lines for the printed mesh, the duration of time to cure light activate the composite resin and the displacement of the printer platform inside the resin. Examples of the 3D printed structures are shown in Figure 12.

## 4. Conclusions

In this work, 3D scaffolds by SLA from AgNPs or AgNWs and an acrylic resin nanocomposite were successfully printed. From the green synthesis, spherical AgNPs with size between 5.9-35.8 nm after 11 h reaction observed by TEM were obtained. Particles size depend on synthesis reaction time. Main functional groups for the nanostructures and nanocomposites were identified by FTIR. The obtained values for thermal diffusivity (D) measured by TL were between 14 and 47x10-8 m2/s for concentrations ranging from 5 to 19x10-5 wt% for the AgNPs. For the AgNWs the D values were between 6 and 37x10-8 m2/s for concentrations ranging from 4 to 17x10-5 wt%. Regarding the characteristic curing time ($\tau$) a maximum of 58 s were obtained for the AgNPs nanocomposites and for the AgNWs nanocomposites maximum was 1651 s for the highest concentration of the nanostructures. Both D and $\tau$ increased with nanostructures concentration. The aim of this work was to find applications of 3D printed scaffolds nanocomposites in the biomedical field.

## Acknowledgement and Funding

We would like to thank CONACYT, COFAA-IPN, EDI for their support.

## References


1. Gibson, I., Rosen, D., & Stucker, B. (2015). *Additive Manufacturing Technologies 3D Printing, Rapid Prototyping and Direct Digital Manufacturing*. ISBN 978-1-4939-2112-6. https://doi.org/10.1007/978-1-4939-2113-3_1

2. Wohlers, T., & Gorne, T. (2014). *History of Additive Manufacturing*. Wohlers Report, Fort Collins, CO: Wohlers Associates, Inc. https://pdf4pro.com/amp/view/history-of-additive-wohlers-report-manufacturing-27057b.html

3. Srivatsan, T.S., & Sudarshan, T.S. (Eds.). (2016). *Additive Manufacturing Innovations, Advances, and Applications*. CRC Press, Taylor & Francis Group, LLC. ISBN-13: 978-1-4987-1478-5.

4. Aghakhanlouy, S., & Grieser, F. 3D Printing Speed: How Fast Do 3D Printers Go in 2023? Updated Jan 25, 2023 https://all3dp.com/2/3d-printer-speed/

5. Currículo e Historial de Litografía y Serigrafía (2010). http://blogdecienciassocialesyhumanas.blogspot.com/search?q=litograf%C3%ADa. Accessed 09 March 2023.

6. Ying, Y., Choong, C., Maleksaeedi, S., Eng, H., Chen, P., & Wei, J. (2017). Curing characteristics of shape memory polymers in 3D projection and laser stereolithography. *Virtual and Physical Prototyping*, 12(1), 77-84. https://doi.org/10.1080/17452759.2016.1254845

7. Gill, A. A. (2012). *Thesis: Applications of Microstereolithography in Tissue Engineering Department of Materials Science and Engineering University of Sheffield.* https://etheses.whiterose.ac.uk/3711/1/Andrew_Gill_Thesis_Final_Submission.pdf Accessed 09 March 2023.

8. Xu, W., Jambhulkar, S., Zhu, Y., Ravichandran, D., Kakarla, M., Vernon, B. *et al.* (2021). 3D printing for polymer/particle-based processing: A review. *Composites Part B: Engineering*, 223 109102. https://doi.org/10.1016/j.compositesb.2021.109102

9. Rosencwaig, A., & Gersho, A. (1976). Theory of the photoacoustic effect with solids. *Journal of Applied Physics*, 47(64), 64-69. https://doi.org/10.1063/1.322296

10. Gosselin, F., Di Renzo, M., Ellis, T. H., & Lubell, W. D. (1996). Photoacoustic FTIR Spectroscopy, a Nondestructive Method for SensitiveAnalysis of Solid-Phase Organic Chemistry. *Journal of Organic Chemistry*, 61(23), 7980-7981. https://doi.org/10.1021/jo961393g

11. Vieyra-Pincel, P., Jiménez-Pérez, J. L., Cruz-Orea, A., Correa-Pacheco, Z. N., & Hernández Rosas, J. (2015). Photoacoustic study of curing time by UV laser radiation of a photoresin. *Thermochimica Acta*, 606, 53-57. https://doi.org/10.1016/j.tca.2014.12.008

12. Rohling, J. H., Medina, A. N., Bento, A. C., Pereira, J. R. D., Rubira, A. F., Baesso, M. L. *et al.* (2001). Differential thermal lens temperature scanning approach to glass transition analysis in polymers: application to polycarbonate. *Journal of Physics D: Applied Physics*, 34, 407-412. https://doi.org/10.1088/0022-3727/34/3/326

13. Cabrera, H., Korte, D., & Franko, M. (2015) Mode-mismatched confocal thermal-lens microscope with collimated probe beam. *Review of Scientific Instruments* 86(053701), 1-7. https://doi.org/10.1063/1.4919735

14. Shen, J., Lowe, R. D., & Snook, R. D. (1992) A model for cw laser induced mode-mismatched dual-beam thermal lens spectrometry. *Chemical Physics*, 165(2-3), 385-396. https://doi.org/10.1016/0301-0104(92)87053-C

15. Stephen, B., Bialkowski, E., & Winefordner, J. D. (Ed). (1996). Photothermal Spectroscopy Methods for Chemical Analysis. *Journal of the American Chemical Society*, 119, 26, 6212. Utah State University. Wiley: New York. ISBN 0-471-57467-8. https://doi.org/10.1021/ja965536s

16. Villegas, O., & Castillo, J. (2018) Study of thermo-optical properties of nanofluids of gold and silver nanoparticles functionalized with polyethylene glycol and sodium dodecyl sulfate in water using thermal lens spectroscopy. Proc. SPIE 10672, *Nanophotonics VII*, 106723S, 1-6. https://doi.org/10.1117/12.2307284

17. Carbajal-Valdez, R., Jiménez-Pérez, J. L., Cruz-Orea, A., Correa-Pacheco, Z. N., Alvarado-Noguez, M. L., Romero-Ibarra, I. C. *et al.* (2017). Thermal properties of centrifuged oils measured by alternative photothermal techniques. *Thermochimica Acta*, 657, 66-71. https://doi.org/10.1016/j.tca.2017.09.014

18. Li, S., Shen, Y., Xie, A., Yu, X., Qiu, L., Zhang, L. *et al.* (2007). Green synthesis of silver nanoparticles using Capsicum annuum L. extract. *Green Chemistry*, 9, 852-858. https://doi.org/10.1039/b615357g

19. Carbajal-Valdéz, R., Rodríguez-Juárez, A., Jiménez-Pérez, J.L., Sánchez-Ramírez, J.F., Cruz-Orea, A., & Correa-Pacheco, Z. N. (2019). Experimental investigation on thermal properties of Agnanowires nanofluids at low concentrations. *Thermochimica Acta*, 671, 83-88. https://doi.org/10.1016/j.tca.2018.11.015

20. Lin, J., Hsueh, Y., & Huang, J. (2014). The concentration effect of capping agent for synthesis of silver nanowire by using the polyol method. *Journal of Solid State Chemistry*, 214, 2-6.
https://doi.org/10.1016/j.jssc.2013.12.017

21. Sun, Y., Gates, B., Mayers, B., & Xia, Y. (2002). Crystalline Silver Nanowires by Soft Solution. *Processing. Nano Letters*, 2(2), 165-168.
https://doi.org/10.1021/nl010093y

22. Socrates, G. (2004). *Infrared and Raman characteristic group frequencies: Tables and Charts*. 3rd Ed. Formerly of Brunel, The University of West London, Middlesex. UK. John Wiley & Sons, Ltd. ISBN 0 470 09307 2.
https://analyticalscience.wiley.com/do/10.1002/sepspec.9780470093078/full/

23. Mahakham, W., Sarmah, A. K., Maensiri, S., & Theerakulpisut, P. (2017). Nanopriming technology for enhancing germination and starch metabolism of aged rice seeds using photosynthesized silver nanoparticles. *Scientific Reports*, 7(8263), 1-21.
https://doi.org/10.1038/s41598-017-08669-5

24. Mehta, B. K., Chhajlani, M., & Shrivastava, B. D. (2017). Green synthesis of silver nanoparticles and their characterization by XRD. *Journal of Physics: Conference Series*, 836(012050), 1-5.
https://doi.org/10.1088/1742-6596/836/1/012050

25. Vanaja, M., & Annadurai, G. (2013) Coleus aromaticus leaf extract mediated synthesis of silver nanoparticles and its bactericidal activity. *Applied Nanoscience*, 3, 217-223.
https://doi.org/10.1088/1742-6596/836/1/012050

26. Mao, H., Feng, J., Ma, X., Wu, C., & Zhao, X. (2012). One dimensional silver nanowires synthesized by self-seeding polyol process. *Journal of Nanoparticle Research*, 14(887), 1-15.
https://doi.org/10.1007/s11051-012-0887-4

27. Rivière, L., Lonjon, A., Dantras, E., Lacabanne, C., Olivier, P., & Rocher Gleizes, N. (2016). Silver fillers aspect ratio influence on electrical and thermal conductivity in PEEK/Ag nanocomposites. *European Polymer Journal*, 85, 115-125.
https://doi.org/10.1007/s11051-012-0887-4

28. Valencia, L. M., Herrera, M., de la Mata, M., Delgado, F. J., & Molina, S. I. (2022). Synthesis of Silver Nanocomposites for Stereolithography: In Situ Formation of Nanoparticles. *Polymers*, 14(6), (1168), 1-14.
https://doi.org/10.1007/s11051-012-0887-4

29. Roberts, A. T., Yang, J., Reish, M., Alabastri, A., Halas, N. J., Nordlander, P. *et al.* (2018). Plasmonic nanoparticle-based epoxy photocuring: A deeper look. *Materials Today*, 27, 14-20.
https://doi.org/10.1007/s11051-012-0887-4